The Journal of Chemical Physics COMMUNICATION scitation.org/journal/jcp

Frequency-dependent hydrodynamic finite size correction in molecular simulations reveals the long-time hydrodynamic tail

Cite as: J. Chem. Phys. 158, 191101 (2023); doi: 10.1063/5.0151406
Submitted: 21 March 2023 • Accepted: 7 April 2023 •
Published Online: 15 May 2023

Laura Scalfi, Domenico Vitali, Henrik Kiefer, and Roland R. Netz[a)]

AFFILIATIONS

Fachbereich Physik, Freie Universität Berlin, Arnimallee 14, 14195 Berlin, Germany

[a)]Author to whom correspondence should be addressed: rnetz@physik.fu-berlin.de

ABSTRACT

Finite-size effects are challenging in molecular dynamics simulations because they have significant effects on computed static and dynamic properties, in particular diffusion constants, friction coefficients, and time- or frequency-dependent response functions. We investigate the influence of periodic boundary conditions on the velocity autocorrelation function and the frequency-dependent friction of a particle in a fluid, and show that the long-time behavior (starting at the picosecond timescale) is significantly affected. We develop an analytical correction allowing us to subtract the periodic boundary condition effects. By this, we unmask the power-law long-time tails of the memory kernel and the velocity autocorrelation function in liquid water and a Lennard-Jones fluid from simulations with rather small box sizes.

With the progress in computational power, molecular dynamics (MD) simulations have become an essential tool to investigate the properties of matter at the microscopic scale. The accessible timescales have not ceased to increase and with them the accuracy of the simulations. However, simulation boxes are still limited to the nanometer scale and delimited, for example, by repulsive walls or more commonly by periodic boundary conditions (PBC). This finite system size introduces constraints and interactions with the walls or other replicas and yields a multitude of static finite-size effects for various observables and phenomena, including surface tension, stress tensors and capillary waves,[1–3] nucleation,[4] phase transitions,[5,6] and critical phenomena.[7,8] Periodicity is particularly relevant for electrostatic interactions:[9] for inhomogeneous systems, significant dipole interactions between replicas occur, which are tackled by the Yeh–Berkowitz dipole correction.[10,11] Dynamic properties also present finite-size effects due to hydrodynamic interactions, which have mostly been investigated in the stationary limit, for example for the thermal conductivity,[12,13] the diffusion coefficient D[14–16] or the friction coefficient $\gamma = k_B T/D$ (with $k_B T$ the thermal energy). Recently, research has shifted toward time (and frequency)-dependent response phenomena to characterize transient and non-equilibrium dynamics in complex systems. Finite-size effects have been found in polymer, glass, or supercooled fluid dynamics, by investigating the time-dependent dynamic structure factor;[17–19] however, studies of the effect of PBC on transient response functions are rare.[20] In this work, we investigate the finite-size dependence of the velocity autocorrelation function (VACF) and of the time-dependent friction function $\Gamma(t)$ (or memory kernel), which quantifies the non-Markovian friction effects in generalized Langevin equations (GLEs). For illustrating our general method, we address the simple case of the position fluctuations of a tagged molecule in a fluid. The associated memory kernels have recently been investigated by using molecular dynamics simulations to bridge the gap between macroscopic hydrodynamics, where the particle is subject to friction, and Hamiltonian dynamics.[21,22] Simulations were compared to hydrodynamic predictions of the friction experienced by a sphere in a fluid. Indeed, hydrodynamic and mode coupling theories predict a negative long-time friction kernel with an asymptotic power-law decay,[21,23–26]

$$\Gamma_{\text{tail}}(t) = -\frac{2\gamma^2}{3\rho}\left[4\pi\left(D + \frac{\eta}{\rho}\right)t\right]^{-3/2}, \tag{1}$$

with ρ being the mass density and η being the shear viscosity of the fluid. The contribution proportional to the diffusion coefficient D comes from the particle diffusion and is often negligible with respect

to the kinematic viscosity η/ρ (see supplementary material Sec. A). Such long-time decay is reflected in the VACF C^{vv}, for which a positive $t^{-3/2}$ decay is predicted.[23–25] The simulation results were found to agree with the predicted power-law decays only for Lennard-Jones (LJ) fluids; instead, a decay of $t^{-5/2}$ was extracted for water and a supercooled fluid.[21,22] Here, we find that the long-time behavior of these time-dependent properties is significantly affected by finite-size effects arising from hydrodynamic interactions with periodic replicas, which masks the predicted long-time tails. Analytic corrections were previously developed in the stationary limit for the diffusion and friction coefficients[27–29] based on the stationary Stokes equation. By extending the calculations of Dünweg *et al.*[14,27] and Yeh and Hummer,[28] we derive a frequency-dependent finite-size correction allowing to retrieve the predicted asymptotic behavior from finite-size simulations. The method developed in this work is also applicable to other kinds of friction responses and more complex coarse-grained coordinates.

In this study, we investigate SPC/E water[30] and a Lennard-Jones (LJ) fluid with parameters corresponding to liquid argon,[31] for which results are shown in supplementary material Sec. B. In both cases, we simulate cubic boxes of length L by using 3D PBC for a range of box lengths L from 1.5 to 5.0 nm (simulation details are provided in supplementary material Sec. A). Figure 1(a) shows a typical snapshot of the water simulation box, alongside a typical trajectory of the x component of a single water molecule (tagged in blue) in Figs. 1(b) and 1(c), at different timescales. Figure 1(c) focuses on the picosecond timescale, which displays ballistic motion, while the nanosecond scale in Fig. 1(b) shows the Brownian diffusive regime. For longer times, the unwrapped water position diffuses away from its initial position.

We consider in this work the Mori GLE[32] for the position of a particle of mass $m = k_B T/\langle v^2\rangle$ with velocity $\vec{v}$, given in the absence of a potential, using the Einstein convention, as

$$m\dot{v}_i(t) = -\int_{-\infty}^{t} \mathrm{d}s\, \Gamma_{ij}(t-s)v_j(s) + F_i^R(t), \tag{2}$$

where the random force F^R has zero mean and is related to the memory kernel Γ by the fluctuation-dissipation theorem $\langle F_i^R(t)F_i^R(0)\rangle = k_B T \Gamma_{ii}(t)$, with $i = x, y, z$. In an equivalent version of the GLE, the lower bound of the integral is zero;[33] we show the equivalence of the two different formulations in supplementary material Sec. C. We introduce here a memory tensor $\Gamma_{ij}(t) = \delta_{ij}\Gamma(t)$, which by isotropy has no off-diagonal components. To extract the memory kernel from simulation trajectories, we use a second-order Volterra iterative scheme[34] (see supplementary material Sec. C), which only depends on the VACF C^{vv}. Figure 1 showcases the kernel extraction from a water simulation: Fig. 1(d) shows C^{vv}, and Fig. 1(e) displays the memory kernel Γ (solid line) and its running integral (dashed line). The integral of the memory kernel links the GLE formalism to the steady-state hydrodynamic picture with a friction coefficient $\gamma = \int_0^\infty \mathrm{d}s\, \Gamma(s)$. Finally, Fig. 1(f) shows the Fourier transform (FT) of the memory kernel, which plays a key role in this work, as we derive the finite-size correction in frequency space. We take the FT of a function $f(\vec{r},t)$ to be $\tilde{f}(\vec{r},\omega) = \int_\infty^{-\infty} \mathrm{d}t\, \mathrm{e}^{i\omega t} f(\vec{r},t)$ and consider for the memory kernel the single-sided FT $\tilde{\Gamma}_+(\omega) = \int_0^\infty \mathrm{d}t \mathrm{e}^{i\omega t}\Gamma(t)$. The real part of $\tilde{\Gamma}_+$ in Fig. 1(f) plateaus for low frequencies and decays to zero for high frequencies, while the imaginary part vanishes both at low and high frequencies.

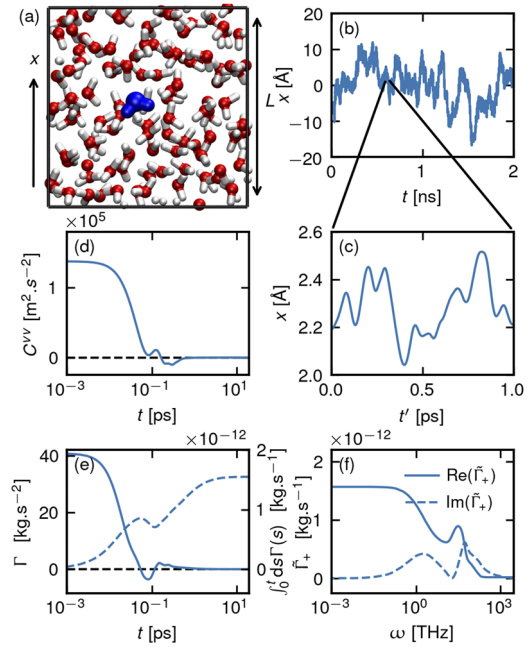

FIG. 1. (a) Snapshot of a cubic simulation box of length L = 1.5 nm filled with SPC/E water molecules. In blue, a single water molecule is highlighted. Position trajectory x of a single water molecule center of mass as a function of time t on the nanosecond (b) and on the picosecond timescale (c). (d) Velocity autocorrelation function C^{vv} averaged over all water molecules in the simulation box as a function of time. (e) Memory kernel Γ (solid line) and integrated friction $\int_0^t \mathrm{d}s\Gamma(s)$ (dashed line). (f) Single-sided Fourier transform (FT) of the memory kernel $\tilde{\Gamma}_+$.

From extensive molecular simulations, we extract memory kernels for different box sizes L ranging from 1.5 to 5 nm. Figures 2(a), 2(c), and 2(e) show the extracted VACF, memory kernels, and kernel integrals for water, respectively. These properties show little variations for short times, while the long-time behavior displays a significant box-size dependence. Note that this long-time regime is particularly susceptible to numerical noise so that the L-dependence is most visible in the integral of the memory kernel in Fig. 2(e), which plateaus at different friction coefficient values γ depending on the box size. The dependence of γ on box size was investigated earlier,[14,27,28] and we verify in supplementary material Sec. D that γ^{-1} is inversely proportional to L with the expected proportionality constant.[28] Most importantly, for the investigated box sizes, we do not observe the long-time tail predicted by Eq. (1), neither for the memory kernels nor for the VACF.

To correct for the effect of PBC on the memory kernel, we start from the transient Stokes equation: the frequency-dependent velocity field $\tilde{v}(\vec{r},\omega)$ due to an external force $\tilde{F}(\vec{r},\omega)$ acting on the fluid is given by a convolution of the force with the tensorial Green's function G. It can be separated into a transverse G^T and a longitudinal G^L contribution, given explicitly both in Fourier and real

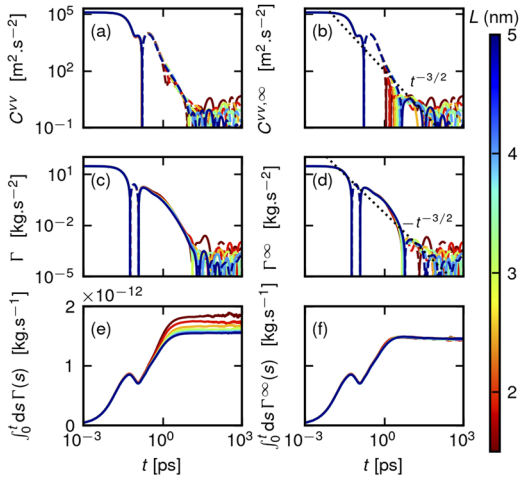

FIG. 2. (a) and (b) Velocity autocorrelation function $C^{vv}(t)$, (c) and (d) memory kernels $\Gamma(t)$, and (e) and (f) integrated friction $\int_0^t ds\Gamma(s)$ for the center of mass position of an SPC/E water molecule in water, for different box sizes $L \in [1.5, 5]$ nm, denoted by different colors, extracted directly from MD simulations (a), (c), and (e) and corrected for finite size effects using Eq. (8) (b) and Eq. (6) (d) and (f). The dashed lines in log–log plots indicate negative values and the data are smoothed by using a Gaussian filter in the log space. The dotted black lines are power-law decays $t^{-3/2}$ as predicted by the long-time tail Eq. (1).

space in Ref. 35 and supplementary material Sec. E. We only need the trace of the Green's functions for the calculation, which are given by

$$\frac{1}{3}\,\mathrm{Tr}\left[\tilde{G}^{T}_{ij}(\vec{r},\omega)\right] = \frac{\mathrm{e}^{-\alpha r}}{6\pi\eta r} \quad \text{and} \quad \frac{1}{3}\,\mathrm{Tr}\left[\tilde{G}^{L}_{ij}(\vec{r},\omega)\right] = \frac{\lambda^2}{\alpha^2}\frac{\mathrm{e}^{-\lambda r}}{12\pi\eta r}, \tag{3}$$

where we introduced two characteristic lengths $\alpha^{-1}(\omega)$ and $\lambda^{-1}(\omega)$,

$$\alpha^2 = \frac{-i\omega\rho}{\eta} \quad \text{and} \quad \lambda^2 = \frac{-i\omega\rho}{4\eta/3 + \zeta + i\rho c^2/\omega}, \tag{4}$$

with ζ being the volume viscosity and c being the speed of sound. In the limit of an incompressible fluid, $c \to \infty$, one has $\lambda \to 0$, and thus, the longitudinal contribution vanishes.

Let us now consider a cubic system of size L with PBC, where we apply a point force at $\vec{r} = \vec{0}$. The force applied in the unit cell has infinitely many periodic images so that the total force field is expressed as $\tilde{F}_i(\vec{r},\omega) = \left[\left(\sum_{\vec{n}} \delta(\vec{r} + \vec{n}L)\right) - 1/L^3\right]\tilde{F}_i(\omega)$, where $\vec{n} = n_x\vec{e}_x + n_y\vec{e}_y + n_z\vec{e}_z$ is a lattice vector with n_x, n_y, n_z integers and $\vec{e}_i$ are the unit vectors in the directions x, y, and z. Note that we added a uniform background force to ensure momentum conservation.[28] The force within the periodic images results in hydrodynamic interactions and induces a spurious velocity field contribution, which depends on the box size and can be written as a convolution of the tensor G and the applied forces. For $\vec{r} = \vec{0}$ and by using the Einstein summation convention, this gives

$$\begin{aligned}\Delta\tilde{v}_i^{\mathrm{corr}}(\omega) &= \int \mathrm{d}\vec{r}'\,\tilde{G}_{ij}(\vec{r}',\omega)\left[\left(\sum_{\vec{n},\vec{n}\neq\vec{0}}\delta(\vec{n}L - \vec{r}')\right) - \frac{1}{L^3}\right]\tilde{F}_j(\omega)\\ &= \left[\left(\sum_{\vec{n},\vec{n}\neq\vec{0}}\tilde{G}_{ij}(\vec{n}L,\omega)\right) - \frac{1}{L^3}\int \mathrm{d}\vec{r}'\,\tilde{G}_{ij}(\vec{r}',\omega)\right]\tilde{F}_j(\omega).\end{aligned} \tag{5}$$

Indeed, $\Delta\tilde{v}_i^{\mathrm{corr}}$ results from the response to the point forces in the periodic images, excluding the central image, and from the background neutralizing force. Next, by introducing the friction kernel extracted from MD simulations $\Gamma^{\mathrm{MD}}(t)$ and the one in the limit of an infinite system $\Gamma^{\infty}(t)$, and using the GLE Eq. (2), we obtain the relationship between the velocity $\Delta\tilde{v}^{\mathrm{corr}}$ and the friction force exerted by the fluid on the tagged particle as $\Delta\tilde{v}_i^{\mathrm{corr}}(\omega) = \left(\left[\tilde{\Gamma}^{\mathrm{MD}}_{+,ij}(\omega)\right]^{-1} - \left[\tilde{\Gamma}^{\infty}_{+,ij}(\omega)\right]^{-1}\right)\tilde{F}_j(\omega)$. By combining this with Eq. (5), the force $\tilde{F}_j(\omega)$ drops out. After taking the trace, we obtain

$$\left[\tilde{\Gamma}^{\infty}_{+}(\omega)\right]^{-1} = \left[\tilde{\Gamma}^{\mathrm{MD}}_{+}(\omega)\right]^{-1} - \Delta\tilde{G}^{\mathrm{corr}}(\omega), \tag{6}$$

where we introduced

$$\Delta\tilde{G}^{\mathrm{corr}}(\omega) = \left[\sum_{\vec{n},\vec{n}\neq\vec{0}}\frac{1}{3}\,\mathrm{Tr}\left[\tilde{G}_{ij}(\vec{n}L,\omega)\right]\right] - \frac{1}{3L^3}\int \mathrm{d}\vec{r}'\,\mathrm{Tr}\left[\tilde{G}_{ij}(\vec{r}',\omega)\right]. \tag{7}$$

This is the main result of this work, which gives an explicit expression for the effect of PBC on the memory kernel and allows us to calculate the infinite box size friction kernel $\Gamma^{\infty}(t)$ from the simulated finite box size kernel $\Gamma^{\mathrm{MD}}(t)$. This frequency-dependent correction can readily be applied to the velocity autocorrelation function C^{vv} (see supplementary material Sec. F) and yields

$$\tilde{C}^{vv,\infty}_{+}(\omega) = \frac{\tilde{C}^{vv,\mathrm{MD}}_{+}(\omega)}{1 + (k_BT)^{-1}\tilde{C}^{vv,\mathrm{MD}}_{+}(\omega)\tilde{\Gamma}^{\infty}_{+}(\omega)\tilde{\Gamma}^{\mathrm{MD}}_{+}(\omega)\Delta\tilde{G}^{\mathrm{corr}}(\omega)}. \tag{8}$$

The mean-squared displacement follows by double integration of $\tilde{C}^{vv,\infty}_{+}$ in the time domain. We further provide explicit forms to compute the transverse contribution to the correction $\Delta\tilde{G}^{T,\mathrm{corr}}$. By using Eq. (3), we explicitly write the transverse correction defined by Eq. (7) as

$$\Delta\tilde{G}^{T,\mathrm{corr}}(\omega) = \frac{1}{6\pi\eta}\left[\sum_{\vec{n},\vec{n}\neq\vec{0}}\frac{\mathrm{e}^{-\alpha|\vec{n}|L}}{|\vec{n}|L}\right] - \frac{2}{3\eta\alpha^2L^3}. \tag{9}$$

For large α, the real space sum in Eq. (9) converges quickly. To cover the low-frequency regime, i.e., for small α, we transform Eq. (7) by using an Ewald summation (for explicit expressions, comparison, and convergence studies, see supplementary material Sec. G). For $\omega \to 0$, we retrieve Yeh and Hummer's zero-frequency correction[28] as expected. Equivalent results are straightforwardly derived for the longitudinal contribution (see supplementary material Sec. H). In the following, we show the results for the hydrodynamic correction with both transverse and longitudinal contributions computed with the Ewald expression.

Figures 2(b), 2(d), and 2(f) present the corrected VACF $C^{vv,\infty}$, memory kernels Γ^{∞}, and memory kernel integrals. All curves from different box sizes fall onto a master curve, as is particularly clear in Fig. 2(f), validating our method to correct these time-dependent

response functions for finite-size effects. In addition, we show in supplementary material Sec. I that using frequency-dependent viscosity spectra $\tilde{\eta}(\omega)$ and $\tilde{\zeta}(\omega)$ extracted from MD simulations results in an even better superposition of the different curves, pointing to a more accurate finite-size correction. Strikingly, our correction modifies the long-time power-law decay of the VACF and the memory kernel. In Fig. 3, we compare the extracted Γ^{MD} for a box length $L = 4$ nm (blue line) and the corrected Γ^{∞} (red line) with the predicted hydrodynamic long-time tail Eq. (1). For long times, $\Gamma^{\mathrm{MD}}(t)$ is positive and decays as $+t^{-5/2}$[22] (blue dotted line). However, this is only a spurious decay due to the PBC: the finite-size correction modifies the kernels at times longer than 1 ps and, as a consequence, reveals the negative long-time tail in Eq. (1) proportional to $-t^{-3/2}$ in the kernels, which results in a decay as $-t^{-1/2}$ of the memory kernel integral for times larger than ~1 ps. The agreement with the analytical prediction Eq. (1) (green dashed line) is excellent. We draw similar conclusions for the VACF and its long-time tail, as shown in Fig. 2 (dotted lines) and in supplementary material Sec. F. The results for an LJ particle in an LJ fluid are given in supplementary material Sec. B and support our conclusions. This demonstrates the importance of considering hydrodynamic interactions due to PBC and correcting time-dependent quantities such as the memory kernel and the VACF when investigating hydrodynamics and long-time behaviors. This correction further allows us to reduce the computational effort and memory (in terabytes) of such studies, and to explore even longer-time behaviors.

Finally, to simplify the use of our frequency-dependent finite-size correction scheme, we introduce an exactly solvable model consisting of concentric spherical shells at a radial separation D, at which constant surface force densities act, as schematized in Fig. 4(d), instead of the cubic periodic lattice considered up until now and drawn in Fig. 4(c). The distance of the innermost spherical shell from the origin is $(1 + m_0)D$, with m_0 being a geometric parameter. This spherical shell model yields a simple functional form,

$$\Delta\tilde{G}^{\mathrm{sph}}(\omega) = \frac{D^2}{3\eta L^3}\left[2f(\alpha^{-1}) + \frac{\lambda^2}{\alpha^2}f(\lambda^{-1}) - \frac{3}{D^2\alpha^2}\right], \qquad (10)$$

where $f(x) = \mathrm{e}^{-m_0 D/x}[e^{D/x}(1 + m_0) - m_0]/(e^{D/x} - 1)^2$ comes from the sum over periodic spheres. The derivation of this expression is given in supplementary material Sec. J, and includes both transverse and longitudinal contributions. We fix the separation D so that the zero-frequency limit equals the Yeh–Hummer expression $D^2 = 3\xi L^2/[\pi(6m_0^2 + 6m_0 + 1)]$, with $\xi = 2.837\,297$, and we fit the parameter m_0 to the numerically determined correction $\Delta\tilde{G}^{\mathrm{corr}}$, yielding $m_0 = 0.387$. Figure 4 shows the comparison of the real part [panel (a)] and imaginary part [panel (b)] of the different corrections derived in this work. The agreement of $\Delta\tilde{G}^{\mathrm{sph}}$ with $\Delta\tilde{G}^{\mathrm{corr}}$ is excellent so that $\Delta\tilde{G}^{\mathrm{sph}}$ can safely be used in practical applications. Interestingly, the transverse contribution is the major part of $\Delta\tilde{G}^{\mathrm{corr}}$, while the longitudinal part is almost negligible, i.e., using only the transverse part of $\Delta\tilde{G}^{\mathrm{corr}}$ is a good approximation. As expected, the real part of the correction retrieves Yeh and Hummer's for zero frequency [horizontal dashed-dotted lines in Fig. 4(a)], and the correction increases in magnitude with $1/L$. Moreover, there is

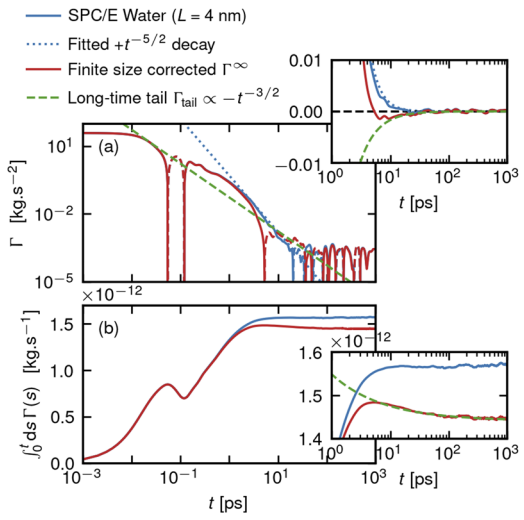

FIG. 3. (a) Memory kernel $\Gamma(t)$ and (b) integrated friction $\int_0^t \mathrm{d}s\Gamma(s)$ for the center of mass position of an SPC/E water molecule in water, extracted from MD simulations (blue line) and corrected for finite-size effects by using Eq. (6) (red line). The dashed lines in log–log plots indicate negative values and the data are smoothed using a Gaussian filter in log space. We show the predicted hydrodynamic long-time tail $\Gamma_{\mathrm{tail}}(t)$ in Eq. (1) (green dashed line), computed using the corrected value of the friction coefficient γ^{∞} (see supplementary material Sec. D) for γ and $D = k_B T/\gamma$, as well as a power-law fit sim $t^{-5/2}$ to the extracted kernel (blue dotted line) suggested by Ref. 22.

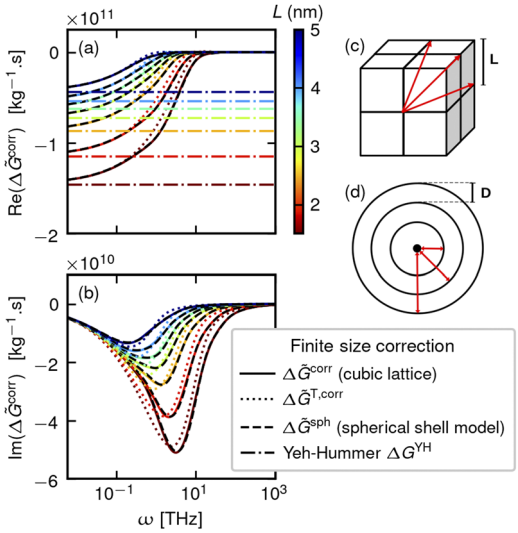

FIG. 4. (a) Real and (b) imaginary parts of the frequency-dependent finite size correction $\Delta\tilde{G}^{\mathrm{corr}}(\omega)$, using the viscosity and density of SPC/E water, for a range of box sizes $L \in [1.5, 5]$ nm, denoted by different colors. We show the total correction including transverse and longitudinal contributions $\Delta\tilde{G}^{\mathrm{corr}}$ in Eq. (7) (solid line), the transverse contribution to the correction $\Delta\tilde{G}^{\mathrm{T,corr}}$ [supplementary material Eq. (G13), dotted lines], and the spherical shell model $\Delta\tilde{G}^{\mathrm{sph}}$ given in Eq. (10) (dashed black lines). For reference, we give the correction derived by Yeh and Hummer in the zero-frequency limit $\Delta G^{\mathrm{YH}} \approx -2.837\,297/(6\pi\eta L)$[28] (horizontal dashed-dotted lines).

a shift toward higher frequencies of the main features of the correction for smaller box lengths L, suggesting that the smaller the box size, the shorter the timescales influenced by hydrodynamic interactions.

The frequency-dependent finite-size correction scheme developed in this work retrieves long-time dynamics, such as the long-time tails predicted by hydrodynamics, from simulations of relatively small systems, which is helpful for MD simulations of aqueous systems and important to encode the correct long-time dynamics, for example, in coarse-grained molecular simulations.[36] This work opens the way to the treatment of more complex systems and observables[37] but could also be extended to other time-dependent transport properties such as electrophoresis, diffusiophoresis, and thermal conductivity.

The supplementary material contains simulation details, results for the Lennard-Jones system, details for the correction of the velocity autocorrelation function, explicit Ewald expressions for the finite-size correction, details on the extraction of and results using frequency-dependent viscosities, and the derivation of the spherical shell model.

We acknowledge support by the ERC Advanced Grant No. 835117 NoMaMemo and by the Deutsche Forschungsgemeinschaft (DFG) via Project No. SFB 1449-431232613-A02. We gratefully acknowledge computing time on the HPC clusters at the Physics department and ZEDAT, FU Berlin.

AUTHOR DECLARATIONS

Conflict of Interest

The authors have no conflicts to disclose.

Author Contributions

Laura Scalfi: Conceptualization (equal); Investigation (equal); Methodology (equal); Supervision (equal); Validation (equal); Visualization (equal); Writing – original draft (equal). **Domenico Vitali**: Investigation (equal); Methodology (equal); Validation (equal); Visualization (equal). **Henrik Kiefer**: Investigation (supporting); Methodology (supporting). **Roland R. Netz**: Conceptualization (equal); Funding acquisition (equal); Methodology (equal); Supervision (equal); Writing - original draft (equal).

DATA AVAILABILITY

The data that support the findings of this study are available from the corresponding author upon reasonable request.

REFERENCES

[1] M. P. Gelfand and M. E. Fisher, "Finite-size effects in fluid interfaces," Physica A **166**, 1 (1990).
[2] M. E. Velázquez, A. Gama-Goicochea, M. González-Melchor, M. Neria, and J. Alejandre, "Finite-size effects in dissipative particle dynamics simulations," J. Chem. Phys. **124**, 084104 (2006).
[3] M. R. Stukan, V. A. Ivanov, M. Müller, W. Paul, and K. Binder, "Finite size effects in pressure measurements for Monte Carlo simulations of lattice polymer models," J. Chem. Phys. **117**, 9934 (2002).
[4] J. Wedekind, D. Reguera, and R. Strey, "Finite-size effects in simulations of nucleation," J. Chem. Phys. **125**, 214505 (2006).
[5] K. Binder, "Finite size effects on phase transitions," Ferroelectrics **73**, 43 (1987).
[6] C. Borgs and R. Kotecký, "Finite-size effects at asymmetric first-order phase transitions," Phys. Rev. Lett. **68**, 1734 (1992).
[7] M. E. Fisher and M. N. Barber, "Scaling theory for finite-size effects in the critical region," Phys. Rev. Lett. **28**, 1516 (1972).
[8] H. G. Ballesteros, L. A. Fernández, V. Martín-Mayor, and A. Muñoz Sudupe, "Finite size effects on measures of critical exponents in $d = 3$ O(N) models," Phys. Lett. B **387**, 125 (1996).
[9] L. M. Fraser, W. M. C. Foulkes, G. Rajagopal, R. J. Needs, S. D. Kenny, and A. J. Williamson, "Finite-size effects and Coulomb interactions in quantum Monte Carlo calculations for homogeneous systems with periodic boundary conditions," Phys. Rev. B **53**, 1814 (1996).
[10] F. Figueirido, G. S. Del Buono, and R. M. Levy, "On finite-size effects in computer simulations using the Ewald potential," J. Chem. Phys. **103**, 6133 (1995).
[11] I.-C. Yeh and M. L. Berkowitz, "Ewald summation for systems with slab geometry," J. Chem. Phys. **111**, 3155 (1999).
[12] P. Chantrenne and J.-L. Barrat, "Finite size effects in determination of thermal conductivities: Comparing molecular dynamics results with simple models," J. Heat Transfer **126**, 577 (2004).
[13] T. Wei, Y. Li, J. Cheng, and C. Jia, "Finite-size effect of the thermal conductivity in one dimensional chain," New J. Phys. **21**, 123003 (2019).
[14] B. Dünweg and K. Kremer, "Molecular dynamics simulation of a polymer chain in solution," J. Chem. Phys. **99**, 6983 (1993).
[15] J. B. Klauda, B. R. Brooks, and R. W. Pastor, "Dynamical motions of lipids and a finite size effect in simulations of bilayers," J. Chem. Phys. **125**, 144710 (2006).
[16] T. J. P. dos Santos, C. R. A. Abreu, B. A. C. Horta, and F. W. Tavares, "Self-diffusion coefficients of methane/n-hexane mixtures at high pressures: An evaluation of the finite-size effect and a comparison of force fields," J. Supercrit. Fluids **155**, 104639 (2020).
[17] B. Dünweg and K. Kremer, "Microscopic verification of dynamic scaling in dilute polymer solutions: A molecular-dynamics simulation," Phys. Rev. Lett. **66**, 2996 (1991).
[18] J. Horbach, W. Kob, K. Binder, and C. A. Angell, "Finite size effects in simulations of glass dynamics," Phys. Rev. E **54**, R5897 (1996).
[19] K. Kim and R. Yamamoto, "Apparent finite-size effects in the dynamics of supercooled liquids," Phys. Rev. E **61**, R41 (2000).
[20] A. J. Asta, M. Levesque, R. Vuilleumier, and B. Rotenberg, "Transient hydrodynamic finite-size effects in simulations under periodic boundary conditions," Phys. Rev. E **95**, 061301 (2017).
[21] D. Lesnicki, R. Vuilleumier, A. Carof, and B. Rotenberg, "Molecular hydrodynamics from memory kernels," Phys. Rev. Lett. **116**, 147804 (2016).
[22] A. V. Straube, B. G. Kowalik, R. R. Netz, and F. Höfling, "Rapid onset of molecular friction in liquids bridging between the atomistic and hydrodynamic pictures," Commun. Phys. **3**, 126 (2020).
[23] B. J. Alder and T. E. Wainwright, "Velocity autocorrelations for hard spheres," Phys. Rev. Lett. **18**, 988 (1967).
[24] B. J. Alder and T. E. Wainwright, "Decay of the velocity autocorrelation function," Phys. Rev. A **1**, 18 (1970).
[25] R. Zwanzig, *Nonequilibrium Statistical Mechanics* (Oxford University Press, Oxford/New York, 2001).

[26]N. Corngold, "Behavior of autocorrelation functions," Phys. Rev. A **6**, 1570 (1972).
[27]B. Dünweg, "Molecular dynamics algorithms and hydrodynamic screening," J. Chem. Phys. **99**, 6977 (1993).
[28]I.-C. Yeh and G. Hummer, "System-size dependence of diffusion coefficients and viscosities from molecular dynamics simulations with periodic boundary conditions," J. Phys. Chem. B **108**, 15873 (2004).
[29]P. Simonnin, B. Noetinger, C. Nieto-Draghi, V. Marry, and B. Rotenberg, "Diffusion under confinement: Hydrodynamic finite-size effects in simulation," J. Chem. Theory Comput. **13**, 2881 (2017).
[30]H. J. C. Berendsen, J. R. Grigera, and T. P. Straatsma, "The missing term in effective pair potentials," J. Phys. Chem. **91**, 6269 (1987).
[31]C. Oostenbrink, A. Villa, A. E. Mark, W. F. Van Gunsteren, "A biomolecular force field based on the free enthalpy of hydration and solvation: The GROMOS force-field parameter sets 53A5 and 53A6," J. Comput Chem. **25**(13), 1656–1676 (2004).
[32]H. Mori, "Transport, collective motion, and Brownian motion," Prog. Theor. Phys. **33**, 423 (1965).
[33]H. K. Shin, C. Kim, P. Talkner, and E. K. Lee, "Brownian motion from molecular dynamics," Chem. Phys. **375**, 316 (2010).
[34]B. Kowalik, J. O. Daldrop, J. Kappler, J. C. F. Schulz, A. Schlaich, and R. R. Netz, "Memory-kernel extraction for different molecular solutes in solvents of varying viscosity in confinement," Phys. Rev. E **100**, 012126 (2019).
[35]A. Erbaş, R. Podgornik, and R. R. Netz, "Viscous compressible hydrodynamics at planes, spheres and cylinders with finite surface slip," Eur. Phys. J. E **32**, 147 (2010).
[36]V. Klippenstein, M. Tripathy, G. Jung, F. Schmid, and N. F. A. van der Vegt, "Introducing memory in coarse-grained molecular simulations," J. Phys. Chem. B **125**, 4931 (2021).
[37]L. Bocquet, J.-P. Hansen, and J. Piasecki, "Friction tensor for a pair of Brownian particles: Spurious finite-size effects and molecular dynamics estimates," J. Stat. Phys. **89**, 321 (1997).